

Yield stresses and flow curves in metallic glass formers and granular systems

Th. Voigtmann^a

Institut für Materialphysik im Weltraum, Deutsches Zentrum für Luft- und Raumfahrt (DLR), 51170 Köln, Germany and
Fachbereich Physik, Universität Konstanz, 78457 Konstanz, Germany and
Zukunftskolleg, Universität Konstanz, 78457 Konstanz, Germany

Received 8 April 2011

Published online: 29 September 2011 – © EDP Sciences / Società Italiana di Fisica / Springer-Verlag 2011

Abstract. We discuss the concept of a glass transition line in the temperature–shear-stress plane in the context of recent simulation data for a metallic melt and dense-packed granular systems. Analyzing these data within a schematic model of the mode-coupling theory for dense glass formers under shear, values for the critical dynamic yield stress (the stress resulting in the limit of arbitrarily slow shear, at the glass transition) are estimated. We discuss two possible scenarios, that of a continuous rise in the dynamic yield stress at the transition, and that of a discontinuous transition, and discuss the data range that needs to be covered to decide between the two cases. A connection is made to the two commonly drawn versions of the jamming diagram, one convex and one concave regarding to the shape of the solid region.

1 Introduction

Dense liquids and in particular glass formers are characterized by slow structural relaxation with a time scale τ that is orders of magnitude slower than that of intrinsic single-particle motion, τ_0 , set for example by the thermal velocity of individual atoms, or the bare self-diffusivity in the case of colloidal suspensions. The so-called α -relaxation time τ depends sensitively on the control parameters such as density or temperature. This slow relaxation makes glass-forming liquids strongly susceptible to external fields and prone to show nonlinear response: the field-induced response time can become fast enough to perturb the structural relaxation, even for moderate applied fields. In the idealized glass state, $\tau \rightarrow \infty$, so that the effect is most extreme here and can be discussed with conceptual clarity. Obviously, the conclusions remain valid *mutatis mutandis* when one assumes τ to be finite, but large enough for practical purposes.

One prominent example of nonlinear effects on dense liquids is their rheology [1]. In the simplest case, one imposes a constant linear shear rate $\dot{\gamma}$ on the system, and observes the resulting shear stress σ . If one assures that the system has reached a steady state, the resulting relation $\sigma(\dot{\gamma})$ is referred to as the flow curve of the system. The steady-state assumption is non-trivial, as the shear flow implies a relaxation time $\mathcal{O}(1/\dot{\gamma})$, and one expects that the time for the system to reach its nonequilibrium steady state is at least of that order if τ is larger. The steady-state

shear stress can then be used to define an apparent viscosity, $\eta(\dot{\gamma}) = \sigma(\dot{\gamma})/\dot{\gamma}$, which for the case of Newtonian liquids is independent of the applied field strength. One expects this to hold also in a slowly relaxing liquid whenever the dressed Péclet number (also called Weissenberg number) $Pe = \dot{\gamma}\tau \ll 1$. Deviations from this expectation are also referred to as non-Newtonian flow. Such nonlinear effects appear if $Pe \gg 1$, even if the bare Péclet number usually used to characterize the strength of the flow, $Pe_0 = \dot{\gamma}\tau_0$, is small, $Pe_0 \ll 1$.

Shear thinning is arguably one of the most common non-Newtonian flow effects; it describes the decrease of the apparent viscosity of the system $\eta(\dot{\gamma})$ with shear rate $\dot{\gamma}$. In the glassy state, it is commonly observed that the applied flow shear melts the system, but does so at the cost of a minimum shear stress, even at the lowest accessible shear rates. In other words, the flow curves $\sigma(\dot{\gamma})$ approach a finite constant in the glass as $\dot{\gamma} \rightarrow 0$. This quantity is termed the dynamic yield stress, σ_y , and is *a priori* different from the static yield stress that indicates the maximum stress that can be applied to the system before force-melting it. The latter would be measured when using the stress as the externally controlled variable instead of the shear rate. If the flow curve is indeed asymptotically constant as $\dot{\gamma} \rightarrow 0$, this implies shear thinning with exponent 1, *i.e.*, the apparent viscosity $\eta \sim 1/\dot{\gamma}$.

Thus, the flow curves in the liquid, $\sigma(\dot{\gamma} \rightarrow 0) \sim \dot{\gamma}$, and in the glass, $\sigma(\dot{\gamma} \rightarrow 0) \rightarrow \sigma_y$, have distinct signatures seen at low shear rates. Further, the range in $\dot{\gamma}$ over which $\sigma \sim \dot{\gamma}$ can be seen, shrinks as one approaches the glass transition from the liquid side by changing the

^a e-mail: thomas.voigtmann@dlr.de

thermodynamic control parameters of the system. Since σ_y increases if one moves deeper into the glassy state, an obvious question is whether the transition in the flow curve at $\dot{\gamma} = 0$ is continuous or discontinuous—*i.e.*, whether the critical dynamic yield stress right at the glass transition $\sigma_y^c = 0$ or $\sigma_y^c > 0$.

The continuous scenario is suggested by theories like the soft-glassy rheology (SGR) model [2], or by analogies to scaling arguments for equilibrium critical points. On the other hand, mode-coupling theory (MCT) for colloidal rheology [3] predicts a discontinuous transition, which it attributes to the appearance of a finite shear modulus on intermediate time scales.

Several authors have suggested scaling forms for the flow curves, or quantities derived from them. Olsson and Teitel [4] suggest a scaling plot for $1/\eta(\dot{\gamma})$ *vs.* $\sigma(\dot{\gamma})$, inspired by their simulations for an athermal granular system where the stress was the externally controlled variable. In particular, they report data collapse for $1/\hat{\eta} = |\epsilon|^{-\alpha}/\eta$ *versus* $\hat{\sigma} = \sigma|\epsilon|^{-\beta}$ onto two master curves, where ϵ is the distance to the critical point distinguishing liquid-like from solid-like states. In the case of the granular system controlled by packing density ρ , $\epsilon = (\rho - \rho_0)/\rho_0$. Liquid states, $\epsilon < 0$, fall onto the master curve $1/\hat{\eta}_-$ that approaches a constant as $\hat{\sigma} \rightarrow 0$, while glassy states, $\epsilon > 0$, are described by $1/\hat{\eta}_+$ that vanishes for finite $\hat{\sigma}$. The critical ($\epsilon = 0$) curve in this picture corresponds to $1/\hat{\eta} \sim \hat{\sigma}^{\alpha/\beta}$ which translates to $\sigma(\epsilon = 0) \sim \dot{\gamma}^x$ with $x = \beta/(\alpha + \beta)$. The values for the scaling exponents were reported to be $\alpha \approx 1.7$ and $\beta \approx 1.2$ [4], from which $x \approx 0.4$ results, although a later refined analysis including corrections to scaling [5] suggests $x \approx 0.3$.

The same scaling has recently been demonstrated to work with data obtained by molecular-dynamics (MD) computer simulations for a model of a metallic glass former, $Zr_{50}Cu_{40}Al_{10}$ [6]. Here, the thermodynamic control parameter varied was the temperature T , so that $\epsilon = (T_0 - T)/T_0$, and the simulations were performed by applying a fixed shear rate, not stress. The scaling exponents reported were $\alpha \approx 1.23$ and $\beta \approx 0.6$, resulting in $x \approx 0.33$.

Such a scaling of flow curves is remarkable since it implies that as $T \rightarrow T_0$ from below, the yield stress continuously vanishes, so that the critical dynamical yield stress is zero, $\sigma_y^c = 0$. In rheological terms, the scaling curves suggested for $\epsilon < 0$ and $\epsilon > 0$ are that of a shear-thinning liquid with $\eta \sim 1/\dot{\gamma}^{1-x}$, and of a power law fluid, respectively. This is incompatible with recent analyses of other shear-thinning glass-forming systems, notably hard-sphere-like colloidal suspensions [7–10]. There, a MCT analysis suggests a non-vanishing critical dynamic yield stress and shear thinning with $\eta \sim 1/\dot{\gamma}$. If true, this would place dense colloidal suspensions in quite a different class of glass formers from the conventional molecular liquids (where temperature rather than density is the dominant control parameter), and the latter (not the former) closer to dense-packed granular systems in their yielding.

Here we reanalyze these recent MD simulation data, and also simulation data for a thermalized granular sys-

tem [11], in terms of a schematic model of mode coupling theory to demonstrate that the finite critical dynamic yield stress, $\sigma_y^c > 0$, predicted by MCT is compatible with these data sets. We address in particular the question on which shear rates need to be reached, and how close one needs to be to the transition in simulation or experiment, in order to decide between the two incompatible scenarios. The analysis indeed hints at a difference between the athermal simulations where the critical-point-like scaling of flow curves was originally proposed, and thermalized glassy systems. We discuss the shapes of the “jamming diagram” [12,13] that are connected to the two cases, both within schematic MCT and some even simpler *ad hoc* flow curves showing shear thinning.

After a brief summary of the schematic MCT model we use (sect. 2), we turn to a discussion of the flow curves and their fits using that model in sect. 3. To highlight the possible difference to the athermal jamming rheology case, we discuss in sect. 4 a variant of the MCT model that can be seen as a toy model for a continuous transition with $\sigma_y^c = 0$. The scaling master curves emerging from this model agree qualitatively with those proposed originally. Finally, in sects. 5 and 6 we turn to the suggestion of constructing a “jamming phase diagram” from the available flow curves, before concluding with sect. 7.

2 Schematic model

The schematic model we use has recently been proposed [14] as an *ad hoc* simplification of a constitutive equation derived from the mode-coupling theory of the glass transition (MCT), extended to the nonlinear response regime in sheared colloidal suspensions via the integration-through transients (ITT) scheme. The ITT-MCT as originally derived [3,15–17] is a microscopic theory, *i.e.*, it describes the macroscopic response σ based on integrals over the microscopic density fluctuation functions, involving coupling coefficients that are given by the equilibrium structure functions of the liquid state. The schematic model replaces these coupling coefficients by a small set of numbers later treated as fit parameters, in order to make computations less unwieldy.

So far a schematic model of ITT-MCT has mostly been discussed in the context of colloidal suspensions, where it has been successful, *e.g.*, in describing both the linear and nonlinear, non-Newtonian rheology of hard-sphere-like suspensions of thermosensitive PNIPAM particles [7–9]. Flow curves for this system have even been described by the full theory within a certain isotropic approximation [10]. Here we are dealing with atomistic systems. The theoretical advantage of implementing Brownian dynamics (without solvent-mediated interactions) in the theory is that this provides an easy, efficient thermostat. In principle, the theory could be derived for a thermostatted Newtonian system, for example by basing it on the SLLD equations [18]. Developments along those lines have recently been presented [19]. Although for the most general case it may be difficult to prove, it may be expected that the features of the nonlinear response that

are governed by the slow relaxation of density fluctuations will be shared among colloidal and atomistic systems, much like the key features of glassy dynamics that are generic. Flow curves obtained from a thermostatted MD simulation of a Lennard-Jones mixture have already been successfully explained with a schematic model [20]. For this reason, and also to highlight a possible connection between the MD results of ref. [6] and colloidal rheology, we continue using the colloidal ITT-MCT.

For the case of interest here, viz., the steady-state response to homogeneous linear simple shear flow of constant rate $\dot{\gamma}$, the model's constitutive equation can be written as

$$\sigma = \dot{\gamma} v_\sigma \int_0^\infty G(\tau; \dot{\gamma}) d\tau. \quad (1)$$

Here, $G(t; \dot{\gamma})$ is the time-dependent transient dynamical shear modulus, depending itself non-trivially on the shear rate $\dot{\gamma}$ in the nonlinear response regime. v_σ is a coupling constant setting the scale for the stresses. In the schematic model, it replaces an anisotropic integral over wave vector space involving the equilibrium static structure functions and shear-advected wave vectors, so that v_σ in fact should depend smoothly on the external control parameters and on shear rate. Following ref. [14], we set $v_\sigma = 100$; note that the schematic model implies stresses in units of the shear modulus. This value gives a good quantitative description of hard-sphere colloidal rheology when the energy and length scales are set by kT and R , a typical particle radius.

The shear modulus displays the slow dynamics typical for the glass transition; its microscopic mode-coupling expression is mimicked by the square of the transient density correlator, $G(t) = \phi^2(t)$, *i.e.*, a correlation function formed by the microscopic densities and involving equilibrium averaging, but the full non-equilibrium time evolution. The latter obeys an integro-differential equation in the steady state,

$$\partial_t \phi(t) + \phi(t) + \int_0^t m(t, t-t') \partial_{t'} \phi(t') dt' = 0, \quad (2)$$

where time is measured in units of the single-particle relaxation time. The memory kernel m incorporates both the cage effect and the suppression of slow dynamics by accumulated strain energy. The model that was suggested in ref. [14] is

$$m(t, t-t') = h(\gamma_{t,0}) h(\gamma_{t,t'}) \times [v_1 \phi(t-t') + v_2 \phi(t-t')^2]. \quad (3)$$

Here, $\gamma_{t,t'} = \int_{t'}^t \dot{\gamma}(\tau) d\tau = \dot{\gamma}(t-t')$ is the strain accumulated between times t' and $t > t'$. The function $h(\gamma) = 1/[1+(\gamma/\gamma_c)^2]$ describes how the retarded coupling of density fluctuations, modeled here by the parameters v_1 and v_2 , is suppressed by shear. The parameter γ_c models the strain needed to break cages and thus reincorporates a length scale information into the schematic model. As in ref. [14], we set $\gamma_c = 0.1$ in agreement with the finding that cages start to yield at strains around 10% [21]. Note that

due to the explicit dependence of m on h and hence the strain, also $\phi(t)$ implicitly depends on the applied flow, so that we indeed can describe nonlinear response.

For $\dot{\gamma} \equiv 0$, the above model reduces to the standard F_{12} model for the description of glassy dynamics around the mode-coupling glass transition [22]. For $\dot{\gamma} = \text{const} \neq 0$ it is a variant of the $F_{12}^{(\dot{\gamma})}$ model used in describing the rheological properties of dense hard-sphere-like PNIPAM suspensions [7–9]. Our model differs by introducing an additional $h(\gamma_{t,0})$ term as was explained in ref. [14]; we adopt the name rheo- F_{12} model for the schematic model defined by eqs. (2) and (3). For steady-state shear flow, the difference between our model and the previously used $F_{12}^{(\dot{\gamma})}$ model is only quantitative [14]. For shear flows with non-trivial time dependence, *e.g.*, step strain tests as discussed within full MCT in ref. [16], the model used here appears to be closer to the microscopic theory. The control parameter space (v_1, v_2) exhibits a glass transition line for $v_2 > 1$, and we imply this restriction from now on. The point given by $v_2^c = 2$, $v_1^c = 2(\sqrt{2}-1)$, yields dynamics whose asymptotic behavior mirrors that of the one found in hard-sphere systems. For simplicity and in line with earlier work on schematic MCT, we introduce a separation parameter ε by $v_1 = v_1^c + h\varepsilon$, $h = 1/(\sqrt{2}-1)$, keeping $v_2 = v_2^c$ constant. In the fits, ε is adjusted to the experimentally varied control parameter —*e.g.*, the temperature T or density ρ . It is then essential that $\varepsilon(T)$, respectively, $\varepsilon(\rho)$, is a smooth function across $\varepsilon = 0$, and linear in the vicinity.

For fixed ε and fixed $\dot{\gamma}$, eqs. (2) and (3) are solved numerically, after which a straightforward integration gives $\sigma(\dot{\gamma}; T)$. Note that the viscosity is always *defined* as $\eta(T) = \sigma(\dot{\gamma}; T)/\dot{\gamma}$, for the steady-state shear rate $\dot{\gamma}$ that corresponds to the given stress σ .

It is known that the schematic-model description is too simplistic to account for the effects setting in at large shear rates, because it embodies only the part arising from structural relaxation. To account for this, the model can be improved by adjusting its high-shear viscosity [7]. For simplicity, we set

$$\sigma_{\text{eff}}(\dot{\gamma}) = \sigma(\dot{\gamma}) + \dot{\gamma} \eta_\infty^0 (1 + \varepsilon). \quad (4)$$

The last term describes a (weakly) density-dependent contribution. For the low shear rates of interest here, this term will make almost no difference, but it can be included to improve the quality of the fits at large $\dot{\gamma}$. For the fits to the metallic-glass simulation, this was found not to be necessary, but we will include a small η_∞^0 correction when later discussing flow curves of granular materials.

3 Results

Figure 1 shows MD simulation data for the inverse shear-thinning viscosity obtained by Guan *et al.* [6] for a model metallic system. Following these authors, the results are shown as a function of shear stress σ , since this is the representation chosen for the scaling plots by Olsson and

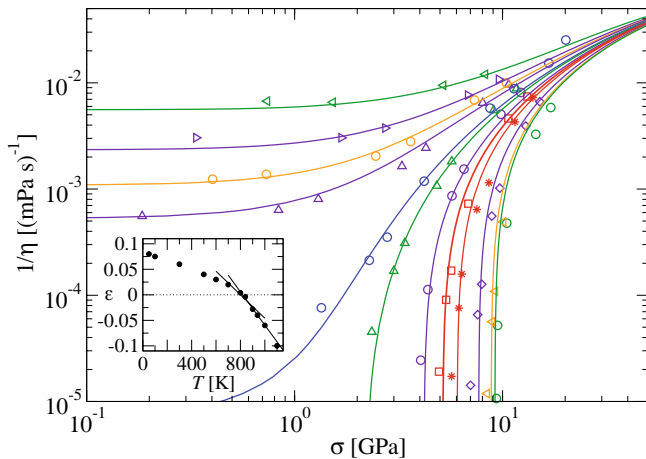


Fig. 1. Inverse shear viscosity $1/\eta$ as a function of steady-state stress σ , for the MD simulation of a metallic melt (symbols; taken and converted from ref. [6]), at $T = 1100$ K, 1000 K, 940 K, 900 K, 840 K, 800 K, 700 K, 600 K, 500 K, 300 K, 100 K, 50 K (top to bottom). Lines are results for a schematic model of mode-coupling theory, with distance parameter $\varepsilon = -0.1, -0.06, -0.04, -0.028, -0.004, 0.004, 0.02, 0.03, 0.04, 0.06, 0.075, 0.1$; shifted by constant factors 8.4 and 4 along the abscissa and ordinate (all other parameters fixed; see text). Inset: relation $\varepsilon(T)$ (circles). Solid lines are linear fits for two different ranges.

Teitel [4]¹. Solid lines in fig. 1 are obtained from the schematic rheo-F₁₂ model of MCT. For simplicity, only a single control parameter was varied, viz., the distance parameter $\varepsilon(T)$ as a function of the simulation temperature (shown in the inset of the figure). To match scales, two shift factors were introduced, $\sigma = s_0 \sigma_{\text{MCT}}$ and $\eta = h_0 \eta_{\text{MCT}}$. We find good agreement using $s_0 = 8.4$ GPa and $h_0 = 0.25$ mPa.s. Our fit procedure is analogous to the one used for a binary Lennard-Jones glass former [20], where a similar $\varepsilon(T)$ curve was found. Note that a more refined fit procedure would include a regular T -dependence in other model parameters as well, possibly leading to even better fits. Still, fig. 1 demonstrates that the data of ref. [6] is fully compatible with the scenario of the schematic model. From the fitted $\varepsilon(T)$, one can construct the corresponding critical temperature by a linear fit around $\varepsilon = 0$. We obtain $T_c \approx (815 \pm 10)$ K, depending on the fit range —*i.e.*, on the assumption over how large a regime the asymptotic behavior $\varepsilon \sim (T_c - T)/T_c$ should hold. This value contrasts somewhat, but is compatible (as we shall see more clearly below) with the singularity temperature $T_0 \approx 860$ K obtained in ref. [6] from the scaling analysis. In the following, we will use the fitted relation $\varepsilon(T)$ shown in the inset of fig. 1 to relate our schematic-model results to realistic temperatures.

The schematic model is incompatible with the scaling idea as outlined above. We thus conclude from the quality

¹ Note that in ref. [6], only scaled values $1/\hat{\eta}$ and $\hat{\sigma}$ are shown, which have been read off from the publication and back-converted here. Units for η have not been given in ref. [6], but σ in GPa and t in ps seems to imply η in mPa.s.

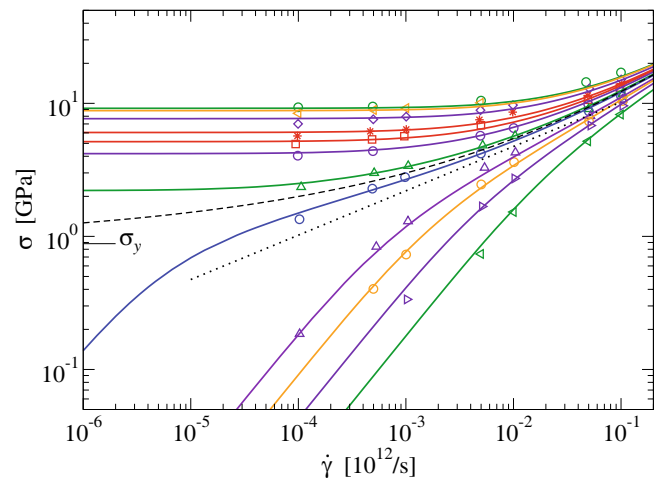


Fig. 2. Same data as in fig. 1, but represented as a flow curve $\sigma(\dot{\gamma})$. The dotted line indicates a power law, $\sigma \sim \dot{\gamma}^{1/3}$. The $T = T_c$ curve from MCT is shown as a dashed line. A short horizontal line indicates the corresponding critical dynamic yield stress, $\sigma_y = \sigma(\dot{\gamma} \rightarrow 0; T = T_c)$.

of our fits and the fact that also the flow-curve scaling appears to work in the fitted regime, as presented in ref. [6], that the available MD data are not conclusive to distinguish a discontinuous yield transition with a dynamical yield stress $\sigma_y > 0$ from a continuous scenario implied by the scaling arguments. We can elaborate this statement further by looking at the data in a representation that puts more emphasis on the behavior at small applied shear rates, $\dot{\gamma} \rightarrow 0$. Figure 2 shows the flow curve, $\sigma(\dot{\gamma})$, extracted from the data shown in fig. 1. This representation also has the advantage that errors are only along the ordinate, since the abscissa represents the variable that is controlled in the simulation.

According to the schematic MCT fit, the curves $\sigma(\dot{\gamma})$ for $T < T_c$ and, crucially, also $T = T_c$, saturate at a finite value as $\dot{\gamma} \rightarrow 0$. We have emphasized this in fig. 2 by including a range of shear rates lower than those accessed in the MD simulation, and also the $\varepsilon = 0$ curve from MCT as a dashed line. The critical-point-like scaling analysis requires $\sigma \sim \dot{\gamma}^{\beta/(\alpha+\beta)}$ as $T \rightarrow T_c$ over an increasing range of $\dot{\gamma}$, with deviations becoming apparent for smaller and smaller $\dot{\gamma}$ the closer one approaches the transition. As mentioned in the introduction, the analysis of ref. [6] is compatible with $\sigma \sim \dot{\gamma}^{1/3}$. This power law is shown as a dotted line in fig. 2. One clearly recognizes the different scenarios predicted by this scaling analysis and the mode-coupling theory. Simulations at lower shear rates would be desirable to better discriminate between them. In particular, it is known within MCT that the asymptotic regime around the yield point is limited to extremely low shear rates [23,24]. In particular, the theory describes the system as a generalized Hershel-Bulkley fluid, $\sigma(\dot{\gamma}) = \sigma_0^0 + \sigma_1^0 |\dot{\gamma}|^m$, but any attempt to extract the exponent m from a limited data set will result in an effective, pseudo-power law exponent. Further, around the inflection point of the theory's $\sigma(\dot{\gamma})$ curves, one can fit effective power laws, whose exponents are close to the

1/3 observed in the critical-scaling analysis, but remain temperature-dependent even as $T \rightarrow T_c$. Coincidentally, even one of the flow curves measured in a hard-sphere-like colloidal suspension of PNIPAM particles in ref. [8], and convincingly fitted with a schematic MCT model, displays a nearly power-law-like $\dot{\gamma}^{1/3}$ growth over three decades in shear rate.

Taking into account the dynamic yield stress calculated within the schematic model, $\sigma_{y,\text{MCT}}^c \approx 0.105$, we obtain for the $\text{Zr}_{50}\text{Cu}_{40}\text{Al}_{10}$ model a critical dynamic yield stress of $\sigma_y^c \approx 0.882$ GPa. Assuming average atomic radii between $R = 1.2 \text{ \AA}$ and 1.5 \AA , which is not unreasonable for this type of metallic system [25], this corresponds to $\sigma_y^c \approx (0.14 \dots 0.26) kT/R^3$. This is close to the values found in a binary Lennard-Jones mixture, [20], and in hard-sphere-like colloidal dispersions, $\sigma_y^c \approx 0.1 kT/R^3$ [9], representative of glass-forming liquids that are dominated by dense, repulsive interactions. Note that at the lowest shear rates available in the MD simulations, the measured stress even at T_c is more than a factor of 2 higher than σ_y^c due to the slow approach to the asymptotic constant.

It is a known limitation of MD simulations for atomistic systems, that the accessible shear rates are rather high: $\dot{\gamma} \geq 10^8/\text{s}$, since the natural unit is $\mathcal{O}(10^{12}/\text{s})$ in fig. 2, a shear rate reached only perhaps in the lubrication of engine parts [1]. Hence, non-Newtonian flow effects are relevant in atomic systems only for low enough temperatures, as one approaches T_c . On the contrary, in soft-matter systems, where natural units are $\mathcal{O}(1/\text{s})$, the kind of flow rates achieved in the simulation are highly relevant for almost all state points. It is instructive to relate the flow rates presented in fig. 2 to dimensionless quantities. To do so, we estimate the thermal velocity $v_{\text{th}} = \sqrt{kT/m} \approx 300 \text{ m/s}$ (using an average atomic mass, and $T \approx T_c$), and hence a time scale $\tau_0 \approx 2R/v_{\text{th}} \approx 1 \text{ ps}$. Thus, in fig. 2 the shear rates span a range from $Pe = 10^{-4}$ to $Pe = 0.1$ in dimensionless Péclet number, which indeed makes them comparable to the colloidal rheology data analyzed with a similar schematic model in refs. [7–9].

The above results can be further related to simulations of sheared granular packings. Both Haxton and Liu [11], and Olsson and Teitel [4, 5] have studied a model system consisting of a 2D equimolar binary mixture of disks with diameters $d = 1$ and $\delta = 1.4$. The density is then expressed as a dimensionless packing fraction φ , defined as the ratio between the disks' volume and the total available volume. In the granular simulations, overlapping disks are taken to repel each other via a harmonic potential, to model elastic deformation of grains. This way, packing fractions ranging from $\varphi = 0.84$ up to $\varphi = 0.9$ could be studied; note that the lower end of this range is already close to the random close packing limit for the hard-disk system, $\varphi_{\text{rcp}} \approx 0.84$. In fact, the glass transition of the same hard-disk mixture has been estimated from simulations to $\varphi_c \approx 0.80$ [26]. Also, the nonlinear rheology under steady shear around the glass transition has been studied extensively [26], and follows the scenario discussed above. A comparison to the full microscopic MCT, which was possible for this system,

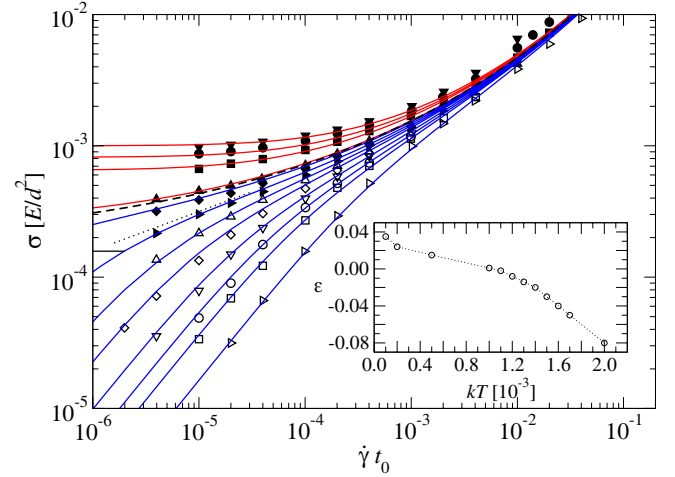


Fig. 3. Flow curve $\sigma(\dot{\gamma})$ from MD simulations of a 2D elastic-disk system, taken from ref. [11] (symbols), for temperatures $T = 0.001, 0.002, 0.005, 0.0010, 0.0011, 0.0012, 0.0013, 0.0014, 0.0015, 0.0016, 0.0017,$ and 0.0020 , from top to bottom, in simulation units E . Shear rates are measured in simulation time units t_0 . Lines are fits using the schematic model, adjusting the distance parameter $\varepsilon(T)$ as shown in the inset, and including an additional large-shear-rate viscosity (see text).

reveals qualitative agreement [26], but also that the theory is in quantitative error regarding the effectiveness of shear to destroy cages. In this light, a schematic-model fit is expected to work well for the hard-sphere colloidal glass transition of the binary mixture. We thus focus on the granular elastic-disk case.

Haxton and Liu [11] have applied a steady strain rate $\dot{\gamma}$ and simulated finite, albeit low, temperatures by integrating the thermostatted SLLOD equations [18]. Hence, the simulation procedure is not unlike the one applied around the glass transition in ref. [26]. One may thus expect qualitatively similar results. Indeed, the resulting flow curves $\sigma(\dot{\gamma})$ are well described by the schematic model of MCT, as shown in fig. 3, where we show the data of ref. [11] together with our fits. These data were taken at $\varphi = 0.9$ for various small temperatures. For the fits, only the distance parameter $\varepsilon(T)$ was adjusted, as shown in the inset of fig. 3. Furthermore, to improve the agreement at large shear rates, $\eta_\infty^0 = 0.1$ was chosen to model the high-frequency viscosity in eq. (4). The stress scale has been adjusted by setting $s_0 = 0.0015$, which accounts for the fact that natural units for the schematic model imply $kT = 1$, whereas the simulations are performed at $kT \approx s_0$, using an energy scale fixed by the harmonic repulsion between overlapping disks. From this fit, a critical temperature of roughly $T_c \approx 0.0010 \pm 0.00005$ is estimated. This is somewhat, but significantly, lower than the critical temperature of 0.0012 estimated by the original authors in ref. [11]. In fig. 3, we highlight this by showing as filled symbols the flow curves that are on the solid-like side of the transition according to the original analysis; a dashed line indicates the $\varepsilon = 0$ solution that separates liquid and solid states in our analysis. The latter lies between states previously identified as solid-like. This happens for the same reason

that our estimated $T_c < T_0$ for the data of Guan *et al.* above: the MCT flow curves allow a description in terms of effective power laws $\sigma \propto \dot{\gamma}^x$ over a certain range in shear rates, slightly on the liquid side of the transition; such power laws are usually taken as indicators for critical behavior. Hence, there typically exists a temperature $T \approx T_0 > T_c$ where power law behavior is seen for some decades in $\dot{\gamma}$; this is highlighted by the dotted lines in figs. 2 and 3.

The above analysis suggests a finite critical dynamic yield stress also for the data of ref. [11], $\sigma_y^c \approx 0.158 kT/d^2$, in reasonable agreement with the results found close to the glass transition at $kT \approx 1$, $\sigma_y^c \approx 0.3 kT/d^2$ [26]. It appears that at these low temperatures, the elastic disks are sufficiently hard to render them hard-sphere-like in their yielding behavior.

Pure power law behavior is not supported by our analysis. While such statements cannot be extracted definitely from data that is available over a finite range of shear rates, the fact that the schematic-model fits work rather well for the cases we investigated so far, is not arbitrary. To see this, we turn to the $T = 0$ data of Olsson and Teitel [4, 5]. In these simulations, only shear-induced overlaps are removed by a diffusive dynamics, and instead of temperature, the density is varied. In ref. [4], the strain rate was further allowed to vary, in an algorithm designed to maintain constant shear stress. Later, the data set was extended for densities closer to the estimated critical point by constant-strain-rate simulations [5]. Both data sets are compatible with each other, with minor (but apparently systematic) deviations discernible for densities above the critical point, which we will ignore for now. They follow the proposed scaling relation $1/\hat{\eta}(\hat{\sigma})$ rather convincingly, although corrections to scaling have to be taken into account in a proper analysis [5].

The scaling argument foresees that the reduced shear stress $\tilde{\sigma} = \sigma/\dot{\gamma}^x$ becomes asymptotically constant at $T = T_c$ as $\dot{\gamma} \rightarrow 0$. Our analysis and the calculations of refs. [23, 24] suggest that data with a non-vanishing critical dynamic yield stress can be confused with such a scaling prediction when looking only at a finite shear rate. To estimate the bound for $\dot{\gamma}$ that must be underrun to distinguish the two cases, we plot in fig. 4 the reduced shear stress obtained from the rheo-F₁₂ model for various distance parameters ε to its transition. It is seen that indeed $\tilde{\sigma}(\dot{\gamma})$ very well approximates a constant for $\varepsilon \approx 0.007$ when setting $x = 0.3$. This holds over at least a decade in shear rates $\dot{\gamma}$, as long as $\dot{\gamma} \gtrsim 3 \times 10^{-6}$ —the regime which concerned the analysis of the available data above. Only for shear rates below $\dot{\gamma} \approx 3 \times 10^{-6}$ (indicated by the shaded area in fig. 4) does one recognize that this constant does not represent a true asymptotic critical power law, but is fortuitous. As expected from above, it furthermore does not hold at $\varepsilon = 0$, but rather for some small negative ε . In fig. 4, some data sets analyzed in fig. 3 are shown again to highlight that they still follow the expectation from the rheo-F₁₂ model.

On the other hand, the data by Olsson and Teitel [5], extending the regime originally probed in their ref. [4] to lower shear rates, does appear to reach into the relevant

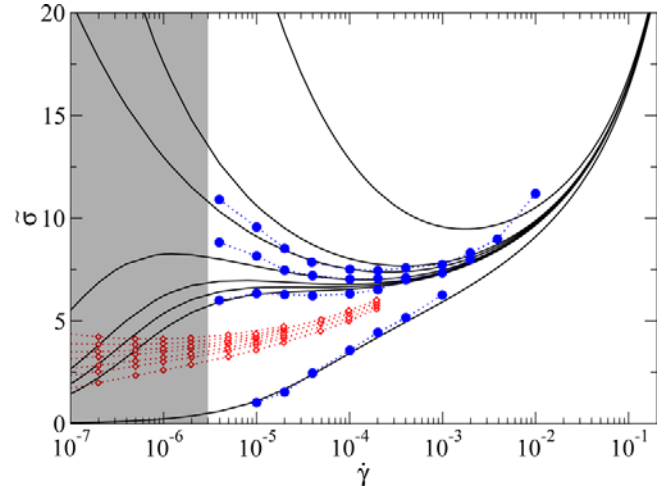


Fig. 4. Reduced shear stress $\tilde{\sigma}(\dot{\gamma}) = \sigma(\dot{\gamma})/\dot{\gamma}^x$ as a function of shear rate $\dot{\gamma}$ for the schematic rheo-F₁₂ model of mode-coupling theory. $x = 0.3$ was chosen. Distance parameters shown are, from top to bottom, $\varepsilon = 0.04, 0.004, 0, -0.008, -0.007, -0.006, -0.004,$ and -0.4 . Filled circles are the data from ref. [11] analyzed in fig. 3 (with the same scaling factor, $s_0 = 0.0015$); only data for $T = 0.0010, 0.0011, 0.0012,$ and 0.0016 are shown for clarity. Diamonds are data from ref. [5], for packing fractions $\varphi = 0.8416, 0.8424, 0.8428, 0.8433, 0.8436, 0.8440,$ and 0.8444 , scaled by $s_0 = 0.002$. The shaded area indicates roughly the region where discontinuous and continuous yield-stress transitions should be distinguishable at small ε .

region; unless one argues for a shift of the relevant units for $\dot{\gamma}$ by a factor of about 100. These data are shown in fig. 4 as diamonds, probing densities rather close to the suspected transition. Coincidentally, the present author found no convincing way of fitting the schematic rheo-F₁₂ model to the data of refs. [4, 5] without making assumptions that appeared implausible. It may be valid to assume that yielding in thermalized systems at $T > 0$ is indeed a qualitatively different phenomenon than the one at $T = 0$ that is envisaged as a critical phenomenon around the “jamming point J ” [12]. Such a distinction has already been hinted at in the scaling analysis [4], and appears to be in line with recent studies of the low- T rheology of amorphous solids [27].

4 Toy model for continuous yielding

Let us elaborate further on the distinction among continuous critical-law-like yielding, and the discontinuous yield-stress transition; in particular, on the effect it has on the flow curves. As is clear from the above, a simple schematic model for the latter is given by MCT’s rheo-F₁₂ model. If we instead set $v_2 = 0$, this results in the rheo-F₁ model. In the quiescent case, this model can be exactly solved [22] and has a continuous liquid-solid transition at $v_1^c = 1$ that is qualitatively different from the standard MCT glass transition. This arises because the memory kernel is no longer a nonlinear functional of the density correlator ϕ , but rather linear. Physically, such a model

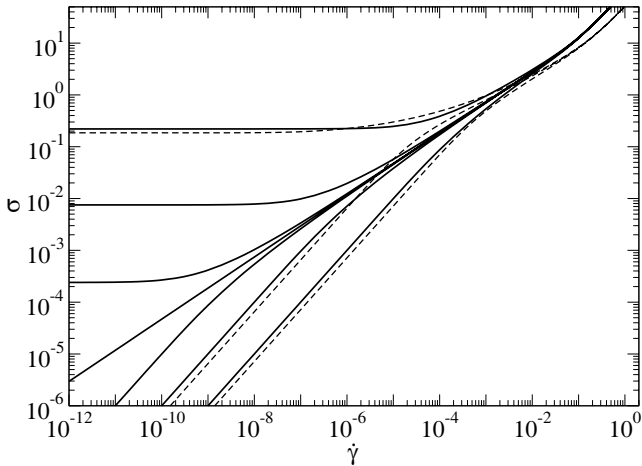


Fig. 5. Flow curves $\sigma(\dot{\gamma})$ for the rheo-F₁ schematic model of mode-coupling theory, exemplifying a continuous dynamic-yield-stress transition. Solid lines show results for distance parameters $\varepsilon = 0.1, 0.01, 0.001, 0, -0.001, -0.01, -0.1$ (top to bottom). Dashed lines show results for the rheo-F₁₂ model (discontinuous transition), for $\varepsilon = 0.001, -0.03, \text{ and } -0.1$.

can be motivated by coupling of density fluctuations to frozen-in disorder. In the F₁ model, the density correlator $\phi(t)$ consequently does not decay via a two-step process involving an intermediate-time plateau, but as a power law, $\phi^c(t) \sim t^{-1/2}$ at the critical point. In combination with steady shear, flow curves result in the rheo-F₁ model that are qualitatively different from those of the rheo-F₁₂ model.

In line with the physical motivation of the F₁ model, it is plausible to assume the relation $G(t) \propto \phi(t)$ in the rheo-F₁ model. Anticipating that a steady shear rate will cut off the critical relaxation on a time scale $\mathcal{O}(1/\dot{\gamma})$, we get $\sigma^c \sim \dot{\gamma} \int_0^\infty t^{-1/2} \exp[-\dot{\gamma}t] dt \sim \dot{\gamma}^{1/2}$ (where we have assumed for simplicity that the shear-induced decay is exponential, although this is not required by the scaling argument). The exponent $x = 1/2$ can be interpreted as a simplistic approximation to the $x \approx 0.3$ claimed in experiment.

Figure 5 shows exemplary flow curves, for various distance parameters $\varepsilon = (v_1 - v_1^c)/v_1^c$. The curve for $\varepsilon = 0$ confirms the power law behavior $\sigma \sim \dot{\gamma}^x$ right at the critical point. It turns out that the shear-induced decay in this model does not precisely scale with $\dot{\gamma}t$ at $\varepsilon = 0$, so that an effective exponent $x \approx 0.6$ results; this power law is visible over about three decades in shear rate at $\varepsilon = \pm 0.001$.

We can compare the flow curves of the rheo-F₁ model exemplified in fig. 5 to the ones obtained from the rheo-F₁₂ model. Results for the latter are shown as dashed lines in fig. 5, with distance parameters ε chosen to roughly match some of the rheo-F₁-model flow curves. (This induces a nonlinear mapping of ε values between the two models.) It can be noted that for sufficiently negative ε , *i.e.*, in the liquid, the two models cannot be qualitatively distinguished. At smaller distances to the transition, the two models give slightly different flow curves that however could possibly not be distinguished in the presence of sta-

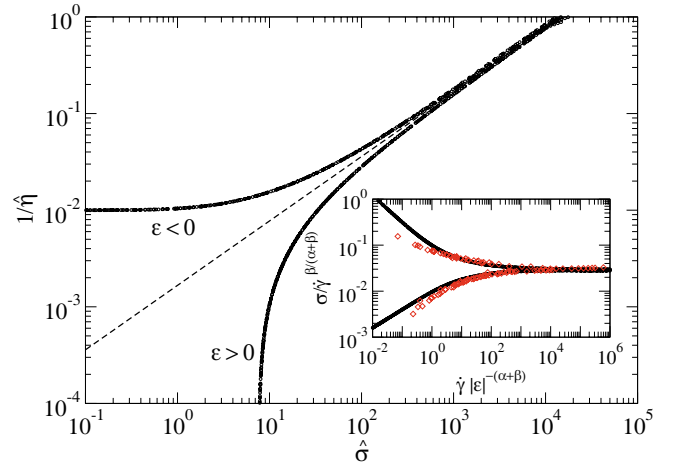


Fig. 6. Scaled inverse viscosity $1/\hat{\eta} = |\varepsilon|^{-\alpha}/\eta$ as a function of scaled stress $\hat{\sigma} = \sigma|\varepsilon|^{-\beta}$ for the rheo-F₁ model, with exponents $\alpha = 1$ and $\beta = 1.5$. The dotted line indicates the power law for $\varepsilon = 0$, with exponent $\alpha/\beta = 2/3$. Inset: reduced stress $\sigma/\dot{\gamma}^x$ as a function of scaled shear rate, $\dot{\gamma}|\varepsilon|^{-(\alpha+\beta)}$. Diamonds are data taken from ref. [4], with exponents as determined there.

tistical noise —compare the $\varepsilon = -0.01$ and $\varepsilon = -0.03$ curves from the two models in fig. 5.

In the glassy state, the two models again give qualitatively similar results, as exhibited by the uppermost pair of curves in fig. 5. This holds, provided ε in the rheo-F₁ model is large enough to result in a dynamic yield stress larger than the minimum one found in the rheo-F₁₂ model, $\sigma_y \geq \sigma_{y,F_{12}}^c$. These simple observations mark the region in $(\varepsilon, \dot{\gamma})$ close to the transition that needs to be entered in order to distinguish the two models. In our example, $-0.03 \leq \varepsilon \leq 0.001$ with respect to the rheo-F₁₂ model, and $\dot{\gamma} \lesssim 10^{-5}$. Taking into account the conversion factors applied in the fit, this corresponds to the two curves closest to T_c in fig. 2, for shear rates that are of the order of $10^7/\text{s}$, just below the ones reached in the simulations of ref. [6]. For the data shown in fig. 3, the statement applies to the four curves just below the critical line marked as dashed, so that we are reasonably sure that at least our continuous-yield-transition toy model, the rheo-F₁ model cannot be used to describe this data. Note that the actual boundaries of the region that allows to distinguish the two cases might depend on the power law exponent x , which is fixed in our toy model.

The flow curves of the rheo-F₁ model exhibit the scaling relation suggested in ref. [4], as shown in fig. 6: the scaled viscosities, $1/\hat{\eta} = |\varepsilon|^{-\alpha}/\eta$, as functions of scaled stress, $\hat{\sigma} = \sigma|\varepsilon|^{-\beta}$ fall on two scaling curves as $\varepsilon \rightarrow 0$, one for $\varepsilon > 0$ and one for $\varepsilon < 0$. At the transition point, a power law holds, $1/\hat{\eta} = \hat{\sigma}^{\alpha/\beta}$. For the scaling plot, we have restricted $-10^{-2} \leq \varepsilon \leq 10^{-3}$, as for larger ε , corrections to scaling would have to be taken into account. Since our toy model is too simplistic, its exponents, $\alpha = 1$ and $\beta = 1.5$, are not in agreement with those determined from the simulation data. However, the shape of the master curves is qualitatively the same. This becomes more apparent if we take out the asymptotic critical power law, *i.e.*, in a plot

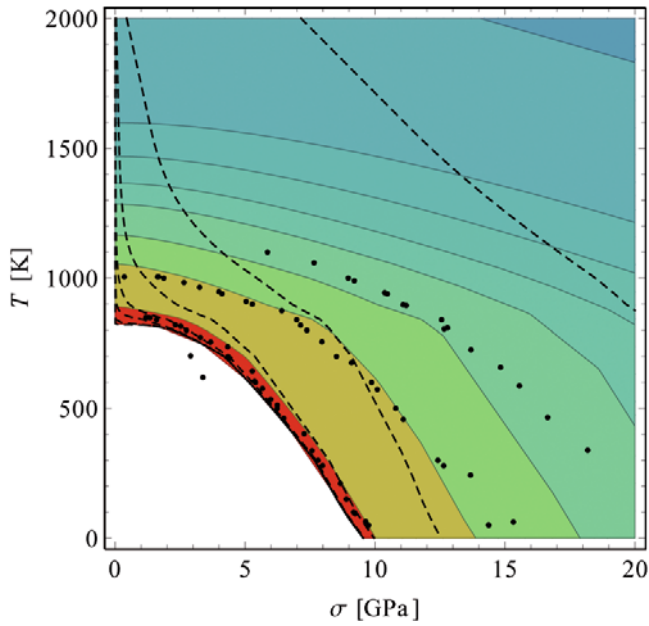


Fig. 7. Lines of constant viscosity $\eta(\dot{\gamma})$ in the stress-temperature plane, represented by solid lines between shaded areas. Viscosity increases exponentially from top to bottom, and right to left. The white area corresponds to the region where $\eta = \infty$. Dashed lines: lines of constant shear rate $\dot{\gamma}$, from 0.01/ps decreasing in powers of ten (right to left). Small circles indicate iso- η lines determined from the original data of ref. [6], scaled as in fig. 1.

of $\sigma/\dot{\gamma}^x$ as a function of scaled shear rate, $\dot{\gamma}|\varepsilon|^{-(\alpha+\beta)}$. Such a plot is shown in the inset of fig. 6, for the rheo-F₁ model together with data taken from Olsson and Teitel, ref. [4]. Note that for this data we are here using the exponents originally determined, but there should be no qualitative change when taking into account the corrected values of ref. [5]. The rheo-F₁₂ model does not admit a scaling for the flow curves as in fig. 6; in light of this, the reported scaling for the MD data in fig. 1 is fortuitous.

5 Jamming diagrams

Even setting the question about a finite or vanishing σ_y^c aside, the construction of a “jamming phase diagram” whose axes comprise temperature and/or density, and the shear stress (as a proxy for a more general external load), is appealing [12, 13]. As a first step, one studies the lines of constant viscosity η in the plane spanned by the control parameter T and the steady-state stress σ . Such a plot has been constructed from MD simulation data for a binary Lennard-Jones glass former by Berthier and Barrat [28]. Recently, such iso-viscosity lines have been extracted from MD simulations for a Zr₅₀Cu₄₀Al₁₀ model [6]. Here we repeat the construction with the schematic model to highlight some generic features of such a representation. Figure 7 shows the iso-viscosity lines for the rheo-F₁₂ model in the (σ, T) plane, where $T(\varepsilon)$ was fixed according to the fit shown in fig. 1. The overall features of this plot are

identical to the one obtained in refs. [28, 6] from the MD data directly, emphasizing that our model indeed gives a faithful representation of such data. The filled circles in fig. 1 are numerical estimates of the iso-viscosity lines based only on the MD data of ref. [6] directly, showing good agreement with those of the rheo-F₁₂ model.

Along the $\sigma = 0$ axis, the iso-viscosity lines trace the equilibrium approach to the glass transition at $(\sigma, T) = (0, T_c)$. The fact that the iso- η lines extend initially horizontally from the $\sigma = 0$ axis in the plot is usually interpreted as signalling that the glass transition is, in the linear-response regime, not perturbed by small stresses. Within the schematic MCT model we find that at constant viscosity, $T(\sigma)|_\eta - T(0)|_\eta \sim \sigma^2$ at small σ . This was also argued for the MD data [6], where it was interpreted as signalling that physical quantities are even functions of the stress due to spatial inversion symmetry. In MCT, it is actually the strain rate—entering quadratically in eq. (3)—that is responsible for the symmetry. This is remarkable since the usual physical interpretation of the steady-shear MCT results involves a shear-induced relaxation time $1/|\dot{\gamma}|$ (giving rise to shear thinning with a thinning exponent -1), implying a different symmetry. This reasoning is however only correct once $|\dot{\gamma}\tau| \gtrsim 1$ [24]. At small σ in the liquid, steady-state shear implies small enough $\dot{\gamma}$. In fact, the iso- $\dot{\gamma}$ lines in the (T, σ) plane at small σ will eventually run perpendicular to the iso- η lines, indicating the true linear response regime. Within the range shown in fig. 7, this limit can only be hinted at. Dashed lines show the calculated lines of constant shear rate; after an initial almost vertical part, they quickly bend over to become almost horizontal over a small range of stresses, $\sigma \lesssim 1$ GPa. This indicates the regime around the yield stress plateau in the liquid, where $\sigma \approx \text{const}$ is not a relevant variable.

At large σ both the iso-viscosity and the iso-shear-rate lines bend over to approach the $T = 0$ axis which they intersect at some finite value, $\sigma_0(\eta)$ for the iso-viscosity lines. The iso- η lines have been reported in ref. [6] to follow a simple master curve, $T/T_0 + (\sigma/\sigma_0)^2 = 1$, where T_0 and σ_0 are the intercepts of a given curve with the respective axes. Within MCT, such a scaling is only approximate, and holds only for a limited viscosity range.

In the plot of the iso-viscosity lines in the (σ, T) plane, there appears a finite region around the origin within which the viscosity remains infinite. This is the region associated with the so-called jammed states in the schematic “jamming diagram” [12]. It should be noted that, although a yield stress is evident from the analysis presented in fig. 2, the value of the critical dynamic yield stress, $\sigma_y^c \approx 1$ GPa, is not readily discernible in fig. 7. The $T \rightarrow 0$ extrapolation of the iso-viscosity lines indeed corresponds to the dynamic yield stress measured at low temperatures, which is almost one order of magnitude larger than the critical value. It should also be noted that the $T \rightarrow 0$ extrapolation is of rather academical value, since quantum effects are not included here. As $T \approx T_c$, the value of σ_y^c is lost in translation from the representation that is more faithful to the way the data are obtained

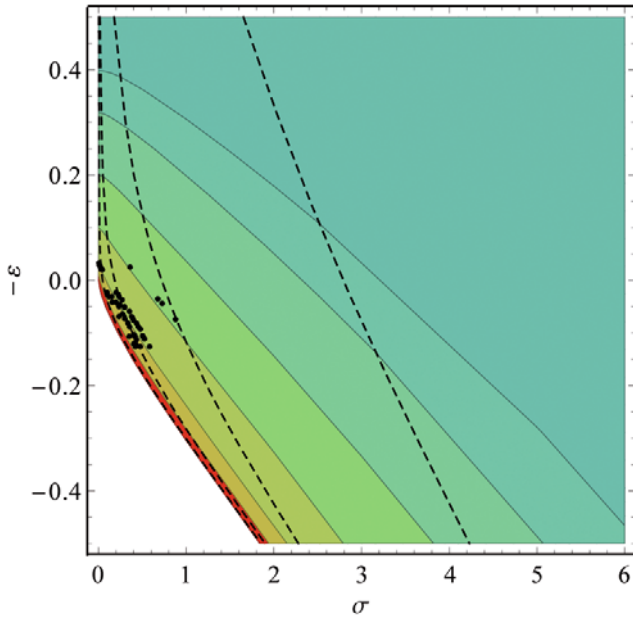


Fig. 8. Lines of constant viscosity $\eta(\dot{\gamma})$ in the plane spanned by the stress σ , and distance parameter ε , for the rheo- F_1 model, analogous to fig. 7. Dashed lines are iso-shear-rate lines from $\dot{\gamma} = 0.01$ to $\dot{\gamma} = 10^{-5}$ (right to left, in powers of ten). Circles indicate estimated iso-viscosity lines from ref. [4]; see text.

(*i.e.*, determining σ as a function of applied $\dot{\gamma}$) into the representation of fig. 7.

This statement is corroborated by constructing the analogous diagram for the rheo- F_1 model with its continuous yield-stress transition. A similar construction of this diagram for a different model involving a continuous yield-stress transition has been given earlier [29]. Since the relation $T(\varepsilon)$ from the fit of fig. 1 is not applicable to the rheo- F_1 model, we instead switch to the plane $(\sigma, -\varepsilon)$, using the distance parameter ε directly. Note that some finite $-\varepsilon_0$ presumably corresponds to $T = 0$. Figure 8 shows the resulting diagram; in qualitative agreement with fig. 7, a region of infinite viscosity emerges around the point $(0, -0.5)$ chosen as the origin of the plot. Noticeable quantitative differences among the two models are the shape of the iso-viscosity lines in the glassy state (for $T < T_c$ or $-\varepsilon < 0$, respectively), and the fact that the initial quadratic dependence on σ of these lines is no longer visible close to $-\varepsilon = 0$ in the rheo- F_1 model. Also shown are estimated iso-viscosity lines from ref. [4]; we have taken $\varepsilon = 4(\varphi - \varphi_c)/\varphi_c$, with $\varphi_c = 0.8415$ for this plot. Unfortunately, the data is only in a rather narrow range, so that we cannot draw strong conclusions from the qualitative similarity to our model’s iso-viscosity lines. Note that in the “jamming diagram” [13], the inverse density $1/\varphi$ would be used as one axis. Within the available data range, this would in fact not change the plot qualitatively. For the rheo- F_1 model, using $1/\varphi \sim 1/v_1$, we would get instead a more noticeably concave region of glassy states around the origin.

Although suggestive, the identification of a “stress-induced glass transition” from fig. 7 (or the fig. 8) is

somewhat misleading. First, it should be noted that even along the lines of constant viscosity, the character of the dynamics changes noticeably. Most prominently, only the $\sigma \rightarrow 0$ limit of the iso-viscosity lines is governed by the equilibrium structural relaxation featuring a stretched-exponential decay. As such, it obeys the time-temperature superposition law known in glass physics as the α -scaling law. Once the shear rate reaches the regime $\dot{\gamma}\tau \gg 1$, α scaling is no longer valid, as the relaxation becomes less stretched. This can be seen in simulation and also in colloidal suspensions [30]. Within MCT, some correlation functions, as for example the transient dynamical shear modulus, even attain “over-relaxation” features where the correlations decay from their intermediate-time plateau not monotonically to zero, but involve a negative dip on the shear-induced time scale [31]. The manifestation of this has been shown to be the ubiquitous stress overshoot seen in startup experiments [21], where a steady shear rate is suddenly applied at some time, and a non-monotonic stress increase is subsequently observed.

Secondly, most calculations discussed here have been performed under applied shear rate, not applied stress. On the shear-molten side of the solid regime in fig. 7, this is likely to be irrelevant in the steady state, although issues may arise at low shear rates [32]. It is known that shear flow is not always homogeneous, and rather shear localization is observed. A non-uniform velocity profile may develop across the sample and lead to the creation of shear bands. There appear to be certain universal mechanisms at work, since shear localization or banding are reported for metallic glasses at low temperatures [33,34], colloidal suspensions [35], as well as granular matter [36], although they may be transient phenomena [37]. Various theoretical approaches exist to address inhomogeneous velocity profiles [38–40], but this is outside the scope of this work. Further, relevant for the solid side of the transition, it is known that under applied load, amorphous materials can undergo creep: their deformation may grow without bound, but sublinearly, resulting in a state that is not strictly solid, but also does not strictly correspond to viscous steady-state flow [1]. This implies that the asymptotic behavior close to the solid-liquid transition line in the (σ, T) plane might change along that line. Hence, the boundary between flowing fluid states and deformed solid ones in fig. 7 will demand further attention beyond the steady-shear case.

6 Generalized Maxwell model

The previous representations of the yield behavior can be understood analytically if one resorts to some simplified constitutive equations modelling the interplay of equilibrium slow dynamics and shear flow. One such model is a generalization of the famous Maxwell model for viscoelastic flow to the nonlinear regime, introduced by Fuchs and Cates [31,41]. While in the original Maxwell model, the viscosity is given by the product of a shear modulus G_∞ and an equilibrium relaxation time τ , $\eta = G_\infty\tau$, the nonlinear Maxwell model replaces τ by an interpolation be-

tween two regimes: for small shear rates, the equilibrium relaxation time still dominates, while for large shear rates, the relaxation is set by $\gamma_c/\dot{\gamma}$. Hence one replaces τ with $(\tau^{-1} + \dot{\gamma}/\gamma_c)^{-1}$. We use in the following a slight modification of this model that incorporates the fact that close to equilibrium, the relaxation time depends quadratically on the strain rate,

$$\sigma(\dot{\gamma}; T) = \dot{\gamma}\eta_\infty + \frac{G_\infty(T)\tau(T)}{[1 + \dot{\gamma}\tau(T)/\gamma_c]^{-1} + \dot{\gamma}\tau(T)/\gamma_c}. \quad (5)$$

In the nonlinear Maxwell model originally proposed, the term in square brackets would be set to unity. The term $\dot{\gamma}\eta_\infty$ models a high-shear-rate viscosity. In the glass the equilibrium (quiescent) relaxation time becomes infinite, $\tau(T) \rightarrow \infty$, so that the nonlinear Maxwell model gives $\sigma(\dot{\gamma}; T < T_c) = \dot{\gamma}\eta_\infty + \gamma_c G_\infty(T)$. Hence, $\sigma_{y, \text{Maxwell}}^c = \gamma_c G_\infty(T_c)$ is the critical dynamic yield stress of the nonlinear Maxwell model.

Solving eq. (5) along an iso-viscosity line, $\dot{\gamma} = \sigma/\eta_0$ with $\eta_0 \geq \eta_\infty$, we see that $\tau(T)$ is determined by a quadratic equation,

$$\tau = -\frac{\gamma_c\eta_0}{2\sigma} + \sqrt{\frac{(\gamma_c\eta_0)^2}{4\sigma^2} + \frac{(\gamma_c\eta_0)^2}{\gamma_c G_\infty \sigma \eta_0 - \sigma^2}}, \quad (6)$$

which yields for small σ the series $\tau = (\eta_0 - \eta_\infty)/G_\infty + (\eta_0 - \eta_\infty)^3/(\gamma_c^2 G_\infty^3 \eta_0^2) \sigma^2 + \mathcal{O}(\sigma^3)$. Assuming $\tau \sim ((T - T_c)/T_c)^{-\alpha}$ for $T > T_c$ (with $\alpha > 0$), we immediately get that $T(\sigma)$ starts as an even function of σ , with a first Taylor coefficient that vanishes as $\eta_0 \rightarrow \infty$. On the other hand, eq. (6) gives $\tau \rightarrow \infty$ for $\sigma = \gamma_c G_\infty \eta_0/(\eta_0 - \eta_\infty)$, and for $\eta_0 \gg \eta_\infty$ this implies $\sigma = \sigma_y^c$. Thus, the iso-viscosity line corresponding to infinite viscosity starts horizontally in the (σ, T) diagram at $(0, T_c)$ and passes through the point (σ_y^c, T_c) . In the nonlinear Maxwell model, there is indeed a discontinuity in the derivative of the iso-viscosity line at that point, because the $T_c(\sigma)$ relation is for $\sigma > \sigma_y^c$ determined by the temperature dependence of $G_\infty(T)$ alone, and no longer $\tau(T)$. In practice, in the more realistic schematic model used above, and at any finite viscosity η_0 , this discontinuity is smoothed, so that σ_y^c is not easily identified from the (σ, T) representation, as discussed above.

For $T < T_c$, we see that $T = G_\infty^{-1}(\sigma - \sigma\eta_\infty/\eta_0)$, where G_∞^{-1} denotes the inversion of the temperature-dependent $G_\infty(T)$. Notably, for vanishing η_∞ , the curves become independent on η_0 ; the spacing of the iso-viscosity lines visible in fig. 7 gives information about the high-shear-rate viscosity. Furthermore, since $G_\infty(T)$ can usually be assumed to be a convex function of temperature, so will be the $T(\sigma)$ iso-viscosity line. This is clearly confirmed in fig. 7.

Let us contrast these features with those of the iso-viscosity lines determined from a similarly simplistic model of power-law-like yielding: we set in the glassy state

$$\sigma(\varepsilon > 0) = \dot{\gamma}\eta_\infty + (\dot{\gamma}/\gamma_c)^x + \varepsilon^\beta, \quad (7)$$

where $\beta > 0$ is the exponent characterizing the increase of the yield stress. We immediately get by using $\varepsilon = 1 - T/T(0)$

$$T/T(0) = 1 - [\sigma(1 - \eta_\infty/\eta_0) - \sigma^x/(\gamma_c\eta_0)^x]^{1/\beta}. \quad (8)$$

Even for $\eta_\infty = 0$, no collapse of iso-viscosity lines is observed here. For very large η_0 , the relation $T/T(0) \sim 1 - \sigma^{1/\beta}$ results. Hence, we expect the scaling exponent β to determine the shape of the iso-viscosity lines in the (σ, T) plane: for $\beta > 1$ one gets a concave glassy region in this representation, while for $\beta < 1$ a convex region results for the glass. Values of $\beta < 1$ will have the tendency to make the diagram resemble more the case obtained from the discontinuous yield-stress transition. This rationalizes why in ref. [6] a value $\beta \approx 0.6 < 1$ had to be assumed. Note that the original scaling analysis by Olsson and Teitel, ref. [4], determined $\beta \approx 1.2 > 1$. The rheo-F₁ model introduced above has $\beta = 1.5$, and results in a concave glassy region for the $(\sigma, -\varepsilon)$ representation, although the effect is weak in fig. 5.

For the ‘‘jamming diagram’’, two schematic pictures can be found in the literature: while the originally suggested glassy region [12] clearly is convex-shaped in the (σ, T) plane, a later version [13] replaces this by a concave-shaped region. It will be interesting to see whether any relation can be established between those two cases and the two cases of discontinuous *versus* continuous transitions for the dynamic yield stress.

7 Conclusion

We have reanalyzed recent simulation results on different glass-forming, respectively jamming systems driven by hard-sphere-like excluded-volume interactions, by fitting a simple schematic mode-coupling theory model for the rheology of dense systems under prescribed shear flow. For both the MD-simulated Zr₅₀Cu₄₀Al₁₀ metallic system [6], and a model of 2D elastic disks mimicking a granular system at low but finite temperature [11], this model gives a quantitative description of the low-shear-rate yielding behavior.

Our analysis implies a finite dynamic yield stress even at the liquid-solid transition, $\sigma_y^c > 0$. In agreement with earlier analyses of hard-sphere-like colloidal suspensions [7–9], two-dimensional thermalized hard-disk mixtures [26], and binary Lennard-Jones glass formers [20], we find that $\sigma_y^c \approx 0.02 \dots 0.1 kT/R^D$ in this class of systems governed by strong steric hindrance among the constituents, where $D = 2$ or $D = 3$ is the dimension of the system. In fact, within the schematic model, this value is related to the value of γ_c , which embodies the typical localization length of a particle in a dense system dominated by hard-sphere-like excluded-volume interactions. This in turn is related to the Lindemann criterion for melting, which states that a solid melts once the single-particle localization length significantly exceeds ‘‘some fraction of’’ the particle diameter [42], typically taken to be 10% or less.

As a corollary, also for the simulated $\text{Zr}_{50}\text{Cu}_{40}\text{Al}_{10}$ metallic system, the physics close to dynamic yielding appears to be dominated by the steric hindrance of the atoms, rather than, say, chemical medium-range order. Certain universal aspects of the nonlinear flow behavior of metallic melts may thus be understood also in simple model systems, such as the widely studied binary Lennard-Jones mixture [28,32], or in colloidal systems.

We are able to estimate the regime of shear rates and distances to the liquid-solid transition one needs to probe in order to discriminate this scenario of a finite critical dynamic yield stress, $\sigma_y^c > 0$, from the one implied by critical-point-like scaling analyses, where $\sigma_y^c = 0$. Current simulations for thermalized hard-sphere-like systems hardly probe this regime, but together with analysis of experiments on colloidal rheology [7–10], a strong case is made for a discontinuous yield-stress transition. The data that to date seem to show the scaling behavior associated with the continuous transition most convincingly [4,5]; these simulations are for an athermal granular system. They indeed probe the relevant regime of low shear rates and small distances to the transition. Simulation data for a similar, slightly thermally agitated system could already be analyzed with our discontinuous-transition scenario, although one would need to probe lower shear rates to decide this case. If true, this would indicate that already small thermal forcing is sufficient to quickly cross over from athermal critical-point-like yielding to a behavior involving a finite critical yield stress not unlike the colloidal one. A more thorough and systematic discussion of temperature effects and the cross-over from $T = 0$ dynamics to the $T \approx T_c$ one remains to be done; with first steps having been taken already [27].

If one only considers moderately small shear rates, $\dot{\gamma} \gtrsim 10^{-5}$ in reduced units, say, scaling relations may appear to work, since the flow curves $\sigma(\dot{\gamma})$ generically are well approximated by power laws over several decades in $\dot{\gamma}$, in the liquid state close to the transition. In light of the above analyses, a strong support for a vanishing critical dynamic yield stress would come from data that shows clear yield-stress plateaus in glassy-state flow curves that are significantly below the value estimated from the relevant length appearing in the Lindemann criterion. Note that the latter will be around 10% of a typical particle diameter mostly for typical dense liquids where excluded-volume interactions dominate. Significantly different localization lengths and hence dynamic yield stress values will arise for, *e.g.*, ultra-soft particles [43], or systems with short-ranged attractions [44].

The representation of the “jamming diagram” constructed via iso-viscosity lines in the (σ, T) plane masks the nature of the critical dynamic yield stress. Even if $\sigma_y^c > 0$, the value cannot be read off from such a diagram. This implies that such a representation is inconvenient to study the yielding behavior under applied shear rate.

We have also studied a toy model for a continuous yield-stress transition, the rheo- F_1 model. In this model, correlation functions do not decay via a two-step relaxation process; even if the shear-induced final relaxation

then follows a scaling with $\dot{\gamma}t$, the constitutive equation gives $\sigma_{y,F_1}^c = 0$. Note that this is not the only possibility to introduce a vanishing critical dynamic yield stress: if one allows for the quiescent critical correlation function to reach a finite plateau, one needs to introduce a mechanism by which the shear-induced decay is not strictly governed by $\dot{\gamma}t$, but also by $\dot{\gamma}$ alone [29]. Note that this requires another, presumably microscopic, time scale to enter in the final relaxation time for dimensional reasons. In this case, again $\sigma_y^c = 0$ would result. Such non-trivial scalings of the shear-induced relaxation times with $\dot{\gamma}$ have been reported [45,30]. However, the observed power-law dependence $\dot{\gamma}^\alpha$ with $\alpha \approx 0.8 \dots 0.9$ over a limited window can also be understood as a pre-asymptotic cross-over to the $\alpha = 1$ expected if the decay is a function of $\dot{\gamma}t$ only, as explicitly demonstrated recently [15]. In general, a study of the dynamical correlation functions under shear, such as the dynamical shear modulus $G(t; \dot{\gamma})$, or the density correlation functions $\phi(t; \dot{\gamma})$, and their scaling with shear rate at the transition point, should be performed for the various systems.

The author acknowledges funding through the Helmholtz-Gemeinschaft (HGF VH-NG 406), the Zukunftskolleg der Universität Konstanz, and from Deutsche Forschungsgemeinschaft (DFG) through the Research Unit FOR1394 “Nonlinear Response to Probe Vitrification”, project P3. This research was supported in part by the National Science Foundation under Grant No. NSF PHY05-51164, during a research visit to the Kavli Institute of Theoretical Physics, Santa Barbara, KITP programme GLASS10 “The Physics of Glasses: Relating Metallic Glasses to Molecular, Polymeric and Oxide Glasses”. This work has been inspired by discussions with K. Samwer, M. E. Cates, T. Egami, and D. Miracle, many of them during the time spent at the KITP.

References

1. R.G. Larson, *The Structure and Rheology of Complex Fluids* (Oxford University Press, 1998).
2. P. Sollich, F. Lequeux, P. Hébraud, M.E. Cates, *Phys. Rev. Lett.* **78**, 2020 (1997).
3. M. Fuchs, M.E. Cates, *Phys. Rev. Lett.* **89**, 248304 (2002).
4. P. Olsson, S. Teitel, *Phys. Rev. Lett.* **99**, 178001 (2007).
5. P. Olsson, S. Teitel, *Phys. Rev. E* **83**, 030302(R) (2011).
6. P. Guan, M. Chen, T. Egami, *Phys. Rev. Lett.* **104**, 205701 (2010).
7. M. Fuchs, M. Ballauff, *J. Chem. Phys.* **122**, 094707 (2005).
8. J.J. Crassous, M. Siebenbürger, M. Ballauff, M. Drechsler, O. Henrich, M. Fuchs, *J. Chem. Phys.* **125**, 204906 (2006).
9. J.J. Crassous, M. Siebenbürger, M. Ballauff, M. Drechsler, D. Hajnal, O. Henrich, M. Fuchs, *J. Chem. Phys.* **128**, 204902 (2008).
10. M. Siebenbürger, M. Fuchs, H. Winter, M. Ballauff, *J. Rheol.* **53**, 707 (2009).
11. T.K. Haxton, A.J. Liu, *Phys. Rev. Lett.* **99**, 195701 (2007).
12. A.J. Liu, S.R. Nagel, *Nature* **396**, 21 (1998).
13. C.S. O’Hern, L.E. Silbert, A.J. Liu, S.R. Nagel, *Phys. Rev. E* **68**, 011306 (2003).

14. J.M. Brader, Th. Voigtmann, M. Fuchs, R.G. Larson, M.E. Cates, Proc. Natl. Acad. Sci. U.S.A. **106**, 15186 (2009).
15. M. Fuchs, M.E. Cates, J. Rheol. **53**, 957 (2009).
16. J.M. Brader, Th. Voigtmann, M.E. Cates, M. Fuchs, Phys. Rev. Lett. **98**, 058301 (2007).
17. J.M. Brader, M.E. Cates, M. Fuchs, Phys. Rev. Lett. **101**, 138301 (2008).
18. D.J. Evans, G.P. Morriss, *Statistical Mechanics of Nonequilibrium Liquids*, 2nd edn. (Cambridge University Press, 2008).
19. S.H. Chong, B. Kim, Phys. Rev. E **79**, 021203 (2009).
20. F. Varnik, O. Henrich, Phys. Rev. B **73**, 174209 (2006).
21. J. Zausch, J. Horbach, M. Laurati, S. Egelhaaf, J.M. Brader, Th. Voigtmann, M. Fuchs, J. Phys.: Condens. Matter **20**, 404210 (2008).
22. W. Götze, *Complex Dynamics of Glass-Forming Liquids* (Oxford University Press, 2009).
23. O. Henrich, F. Varnik, M. Fuchs, J. Phys.: Condens. Matter **17**, S3625 (2005).
24. D. Hajnal, M. Fuchs, Eur. Phys. J. E **28**, 125 (2009).
25. D.B. Miracle, D.V. Louzguine-Luzgin, L.V. Louzguina-Luzgina, A. Inoue, Int. Mater. Rev. **55**, 218 (2010).
26. O. Henrich, F. Weysser, M.E. Cates, M. Fuchs, Philos. Trans. R. Soc. A **367**, 5033 (2009).
27. J. Chattoraj, C. Caroli, A. Lemaître, Phys. Rev. Lett. **105**, 266001 (2010).
28. L. Berthier, J.L. Barrat, J. Chem. Phys. **116**, 6228 (2002).
29. L. Berthier, J.L. Barrat, J. Kurchan, Phys. Rev. E **61**, 5464 (2000).
30. R. Besseling, E.R. Weeks, A.B. Schofield, W.C.K. Poon, Phys. Rev. Lett. **99**, 028301 (2007).
31. M. Fuchs, M.E. Cates, Faraday Discuss. **123**, 267 (2003).
32. F. Varnik, L. Bocquet, J.L. Barrat, J. Chem. Phys. **120**, 2788 (2004).
33. C.A. Schuh, T.C. Hufnagel, U. Ramamurty, Acta Mater. **55**, 4067 (2007).
34. Y. Shi, M.B. Katz, H. Li, M.L. Falk, Phys. Rev. Lett. **98**, 185505 (2007).
35. R. Besseling, L. Isa, P. Ballesta, G. Petekidis, M.E. Cates, W.C.K. Poon, Phys. Rev. Lett. **105**, 268301 (2010).
36. D. Fenistein, M. van Hecke, Nature **425**, 256 (2003).
37. T. Divoux, D. Tamarii, C. Barentin, S. Manneville, Phys. Rev. Lett. **104**, 208301 (2010).
38. M.L. Manning, J.S. Langer, J.M. Carlson, Phys. Rev. E **76**, 056106 (2007).
39. S.M. Fielding, M.E. Cates, P. Sollich, Soft Matter **5**, 2378 (2009).
40. G. Ovarlez, S. Rodts, X. Chateau, P. Coussot, Rheol. Acta **48**, 831 (2009).
41. M. Fuchs, M. Ballauff, Coll. Surf. A **270–271**, 232 (2005).
42. F.A. Lindemann, Phys. Z. **11**, 609 (1910).
43. C. Mayer, E. Zaccarelli, E. Stiakakis, C.N. Likos, F. Sciortino, A. Munam, M. Gauthier, N. Hadjichristidis, H. Iatrou, P. Tartaglia *et al.*, Nat. Mater. **7**, 780 (2008).
44. K.N. Pham, G. Petekidis, D. Vlassopoulos, S.U. Egelhaaf, P.N. Pusey, W.C.K. Poon, Europhys. Lett. **75**, 624 (2006).
45. J.L. Barrat, L. Berthier, Phys. Rev. E **63**, 012503 (2000).